Pharmacogenomics and Personalized Medicine

Dovepress
Taylor & Francis Group

Open Access Full Text Article

ORIGINAL RESEARCH

Berberine Repairs Intestinal Mucosal Barrier by Targeting HSP90AA1 and MAPK14

Danya Zhao[1,*], Yang Zhai[2,*], Chen Chen[3,*], Junkang Chen[4], Dongya Chen[1], Qiang Yang[5], Zhexuan Yu[3], Shisi Shao[3], Yao Huang[3], Jianlong Shu[2]

[1]Department of Gastroenterology, Hangzhou Red Cross Hospital/Hospital of Integrated Chinese and Western Medicine, Hangzhou, People's Republic of China; [2]Department of Chinese Medicine, Seventh People's Hospital of Nanning, Nanning, People's Republic of China; [3]The First School of Clinical Medicine of Zhejiang Chinese Medical University, Hangzhou, People's Republic of China; [4]Department of Gastroenterology, Pujiang County Hospital of Traditional Chinese Medicine, Jinhua, People's Republic of China; [5]Hangzhou TCM Hospital Affiliated with Zhejiang Chinese Medical University, Hangzhou, People's Republic of China

*These authors contributed equally to this work

Correspondence: Jianlong Shu, Email jianlong0214@yeah.net

Pharmacogenomics and Personalized Medicine downloaded from https://www.dovepress.com/
For personal use only.

Background: Berberine (BBR), a key compound in Coptis chinensis, has broad pharmacological properties, though its specific Crohn's disease (CD) targets and mechanisms are undefined.

Materials and Methods: We employed network pharmacology, mendelian randomization (MR), molecular docking, and molecular dynamics simulations to identify potential target genes. Next, we assessed the efficacy of BBR in vitro and in vivo.

Results: HSP90AA1 and MAPK14 were identified as potential target genes of BBR in the treatment of CD. In vitro experiments revealed that BBR downregulated LPS-induced HSP90AA1, MAPK14, and TNF-α while restoring tight junction proteins (ZO-1, Occludin, Claudin-1, JAM-A). Both HSP90AA1 inhibitor (17-AAG) and MAPK14 inhibitor (SB203580) significantly mitigated the reduction in ZO-1, Occludin, Claudin-1, and JAM-A expression caused by LPS. Furthermore, in vivo experiments revealed that BBR treatment effectively alleviated weight loss, the disease activity index (DAI), and colon shortening in a model of DSS-treated mice. BBR also ameliorated pathological changes in the colon, repaired goblet cells, reduced the expression of HSP90AA1, MAPK14, and TNF-α, and increased the expression of ZO-1, Occludin, Claudin-1, and JAM-A.

Conclusion: BBR inhibits the expression of HSP90AA1 and MAPK14 both in vitro and in vivo, thereby facilitating the repair of the intestinal mucosal barrier.

Keywords: Crohn's disease, berberine, Mendelian randomization, molecular dynamics, experimental validation

Crohn's disease (CD), a form of inflammatory bowel disease (IBD), is driven by intestinal mucosal barrier dysfunction. This impairment facilitates microbial translocation and disrupts immune homeostasis, leading to a Th1/Th17-polarized inflammatory response marked by elevated TNF-α and IL-17, alongside reduced regulatory T-cell (Treg) activity.[1] Chronic inflammation promotes progressive tissue damage, resulting in complications such as strictures, fistulae, abscesses, and increased colorectal cancer risk.[2]

Tight junctions (TJs) are apical intercellular complexes in epithelia that control paracellular permeability and protect against luminal pathogens and toxins. These complexes consist of key proteins including the scaffolding organizer ZO-1, the transmembrane proteins Occludin and Claudin-1, and the immunoglobulin superfamily member JAM-A. Together, they form a selective barrier that regulates ion transport and prevents macromolecule passage across the intestinal epithelium.[3–7]

Coptis chinensis—derived from the dried rhizomes of Coptis chinensis Franch. Coptis deltoidea C.Y. Cheng et Hsiao, and Coptis teeta Wall—is a canonical traditional Chinese medicine used to treat damp-heat syndrome, particularly gastrointestinal disorders such as diarrhea. Its therapeutic efficacy is attributed to berberine (BBR), a benzylisoquinoline alkaloid with pleiotropic immunomodulatory properties. BBR undergoes extensive metabolism in vivo, however, research findings indicate that the predominant biological activity is attributed to the parent compound BBR itself.[8] BBR exerts protective effects in the

Received: 16 June 2025
Accepted: 3 November 2025
Published: 15 November 2025

© 2025 Zhao et al. This work is published and licensed by Dove Medical Press Limited. The full terms of this license are available at https://www.dovepress.com/terms.php and incorporate the Creative Commons Attribution – Non Commercial (unported, v4.0) License (http://creativecommons.org/licenses/by-nc/4.0/). By accessing the work you hereby accept the Terms. Non-commercial uses of the work are permitted without any further permission from Dove Medical Press Limited, provided the work is properly attributed. For permission for commercial use of this work, please see paragraphs 4.2 and 5 of our Terms (https://www.dovepress.com/terms.php).

colon by preserving the structure and function of the intestinal mucosal barrier and modulating intestinal mucosal immune homeostasis, mediated through the Wnt/β-catenin signaling pathway.[9] These multi-target actions highlight BBR's potential in managing CD through immunomodulation and barrier protection, though further research is needed to fully elucidate its mechanisms and clinical efficacy.

This study employed a multi-methodological approach—integrating network pharmacology, mendelian randomization (MR), molecular docking, and experimental validation—to elucidate the therapeutic mechanism of BBR in CD. Our results not only decipher the mechanistic basis of BBR's effects but also identify HSP90AA1 and MAPK14 as novel, druggable targets. Targeting this axis presents a promising dual-target therapeutic strategy for developing new treatments for CD aimed at restoring intestinal barrier function and mitigating inflammation.

Materials and Methods

Collection of Chemical Component Targets of BBR

Pharmacophore modeling is a widely utilized ligand-based approach for drug target identification.[10] First, the selected structure file of the BBR was downloaded from the PubChem database (https://pubchem.ncbi.nlm.nih.gov/). Subsequently, the structural data was imported into PharmMapper (www.lilab-ecust.cn/pharmmapper) for target prediction. To obtain target information, gene name conversion in UniProt (https://www.uniprot.org) was performed to identify potential targets of the chemical components.

Screening of BBR Therapeutic Targets for CD

Using "Crohn's disease" as the keyword, the GeneCards database (https://www.genecards.org/) was searched to obtain the disease targets associated with CD and establish a dataset of these targets. R version 3.6.3 was used to construct a Venn diagram to identify potential targets for the effects of BBR.

Unveiling Core Regulatory Modules and Functional Enrichment Analysis

The protein-protein interaction (PPI) network was performed using STRING (https://string-db.org/), applying a confidence level threshold of >0.4. The protein interaction relationships were subsequently imported into Cytoscape software (version 3.7.1), and the MCODE plug-in was utilized to identify modules within the protein interaction network, with a degree cutoff=2, score cutoff=0.2, k-core=2, and max.depth=100, which were used as screening parameters to visualize the key BBR targets for treating CD. Gene Ontology (GO) functional analysis and and Kyoto Encyclopedia of Genes and Genomes (KEGG) pathway enrichment analysis were conducted via R version 3.6.3. The ggplot2 package was utilized for visualization, enabling the identification of possible biological processes and signaling pathways through which BBR may exert its therapeutic effects in treating CD.

MR Analysis to Screen Exposure Genes for CD Pathogenesis

The genome-wide association study (GWAS) data for CD were sourced from the FinnGen Consortium (Release R10, https://www.finngen.fi/en/access_results). We selected the genetic instruments corresponding to the expression quantitative trait loci (eQTLs) of the aforementioned gene targets.

Initially, we utilized eQLTgen (https://eqtlgen.org/cis-eqtls.html) to map the protein target to the associated SNP. In this study, we employed the following criteria for selecting instrumental variables: (i) Given the challenges in identifying protein instrumental variables that overlap with disease GWAS at the locus, we established a screening threshold of $P < 5\times10^{-8}$ for protein SNPs; (ii) For each protein, we retrieved the locus information from the National Center for Biotechnology Information (NCBI) (http://www.ncbi.nlm.nih.gov), as detailed in Table 1, subsequently mapping the protein SNP to the corresponding locus ±100 kb; (iii) $r^2 < 0.001$ was set as the criterion for independence testing; (iv) the F statistic ($F = R^2 \times (N - 2)/(1 - R^2)$) was employed to assess the strength of the instrumental variables, with an F value exceeding 10 being deemed acceptable During the data analysis phase, we utilized the "TwoSampleMR" R package for MR analysis. For proteins with multiple instrumental variables, we primarily applied the inverse variance weighting (IVW) method to evaluate the effect size of the protein on CD; conversely, for proteins with only a single instrumental variable, we employed the Wald ratio method.

Table 1 Locus Information of Potential Targets for BBR for CD

Ids	Genes	GeneChr	GeneStart	GeneEnd
eqtl-a-ENSG00000100985	MMP9	20	44,637,547	44645200
eqtl-a-ENSG00000080824	HSP90AA1	14	102,547,079	102606086
eqtl-a-ENSG00000082701	GSK3B	3	119,540,168	119813294
eqtl-a-ENSG00000164111	ANXA5	4	122,589,101	122618135
eqtl-a-ENSG00000164305	CASP3	4	185,548,850	185570601
eqtl-a-ENSG00000132170	PPARG	3	12,328,867	12475843
eqtl-a-ENSG00000196396	PTPN1	20	49,126,920	49201778
eqtl-a-ENSG00000112062	MAPK14	6	35,995,585	36079013
eqtl-a-ENSG00000140443	IGF1R	15	99,191,768	99507759
eqtl-a-ENSG00000161570	CCL5	17	34,198,495	34207364
eqtl-a-ENSG00000169032	MAP2K1	15	66,679,250	66783882
eqtl-a-ENSG00000091831	ESR1	6	151,977,807	152450754
eqtl-a-ENSG00000197122	SRC	20	35,973,102	36034453
eqtl-a-ENSG00000186951	PPARA	22	46,546,429	46639652
eqtl-a-ENSG00000115415	STAT1	2	191,833,875	191878897
eqtl-a-ENSG00000163631	ALB	4	74,270,004	74,287,199

Molecular Docking and Molecular Dynamics Simulation

The chemical structure of the BBR was retrieved from PubChem and optimized in Chem 3D (v22.0.0.22) via the MMFF94 module. The relevant protein structure was sourced from RCSB PDB (https://www.rcsb.org/). Schrödinger Maestro (v11.1.011) was then used to predict docking sites, and LigDock was used to simulate compound–protein interactions.

Additionally, molecular dynamics analysis was performed on the substrate with the top docking score to assess binding stability. This analysis was executed with GROMACS 5.1.4,[11,12] which uses the Amber 99Sb-ILDN force field and TIP3P water model for the Ply206CBD protein, and ACPYPE for ligand topology.[13] Each molecular dynamics system was simulated for 100 ns at 310 K and 1 bar. The root-mean-square deviation (RMSD) and root-mean-square fluctuation (RMSF) values were calculated via GROMACS tools.

Cell Culture

This study utilized Caco-2 cells, a human colon adenocarcinoma-derived line exhibiting mature enterocyte traits, obtained from the ATCC and verified for short tandem repeat (STR) and mycoplasma-free status. These cells were cultured in RPMI 1640 (Sigma–Aldrich, USA) supplemented with 20% FBS (Biological Industries, USA) and 100 U/mL penicillin–streptomycin (Gibco, USA) at 37°C in a 5% CO_2 incubator. Stimulation was achieved with (Sigma–Aldrich, USA), 17-AAG (HSP90AA1 inhibitor, S86426, Yuan Ye, Shanghai, China), SB203580 (MAPK14 inhibitor, T92668, Yuan Ye, Shanghai, China), and Berberine (T92401, Yuan Ye, Shanghai, China).

Cell Counting Kit-8 (CCK-8) Assay

Caco-2 cells (1 × 10^4) were plated into 96-well plates to achieve 80% confluency and subsequently incubated with BBR at concentrations of 0, 5, 10, 20, 40, and 80 μM for 24 hours. Following this incubation, 10 μL of CCK-8 (Dojindo, Japan) reagent was added to each well, and the absorbance of the cells was measured at 450 nm after an additional 2 hours of incubation.

Enzyme-Linked Immunosorbent Assay (ELISA)

After cell injury was induced with LPS, BBR-supplemented medium was added for 24 hours. The cells treated with trypsin were centrifuged at 3000 rpm and 4°C for 10 minutes. A TNF-α ELISA kit from Jiangsu Enzyme Immune Industrial Co., Ltd., was used following the manufacturer's protocol.

Animal Experiments and Dosage Information

Animal experiments were designed according to ARRIVE 2.0 Guideline. A total of 40 male C57BL/6 mice aged 9–12 weeks were purchased from Shanghai Slac Laboratory Animal Co. Ltd (Shanghai, China) (permission number: SCXK (hu) 2022–0004). The mice were cultured under standard conditions (temperature of 20–26°C, relative humidity of 40–70%, light-dark cycle of 12/12 h, clean bedding, free access to water, and standard dry pellet diet). After a week of adaptive feeding, the mice were randomly divided into five groups, with eight mice in each group. In this study, we used dextran sulfate sodium (DSS) mice, a well-established mouse model for studying colitis resembling CD.[14] DSS was purchased from MP Biomedicals (DSS, MP Biomedicals, MW 47,000, California, USA), and BBR was purchased from Shanghai Yuan Ye Biotechnology Co. Ltd. (Shanghai, China).

The groups were as follows: 1) normal group, continually fed water alone for 7 days; 2) model group, colitis was induced by administering 2% DSS in drinking water for 5 days, with concurrent daily intragastric gavage of normal saline, followed by regular drinking water for the next 2 days; 3) BBR-L (Low dose), colitis was induced by administering 2% DSS in drinking water for 5 days, with concurrent daily intragastric gavage of BBR (20 mg/kg), followed by regular drinking water for the next 2 days; 4) BBR-M (Medium dose) group, colitis was induced by administering 2% DSS in drinking water for 5 days, with concurrent daily intragastric gavage of BBR (40 mg/kg), followed by regular drinking water for the next 2 days; 5) BBR-H (High dose), colitis was induced by administering 2% DSS in drinking water for 5 days, with concurrent daily intragastric gavage of BBR (80 mg/kg), followed by regular drinking water for the next 2 days. The disease activity index (DAI) was calculated on the basis of body weight change, stool consistency, and gut bleeding. On day 8, the mice were euthanized with isoflurane.

Animal studies were performed according to the NIH Guide for the Care and approved by the Ethics Committee of Zhejiang Traditional Chinese Medical University (IACUC-202505-01).

H&E and AB-PAS Staining

On day 8, the mice were euthanized with isoflurane. Colon tissues were removed and prepared by rinsing with PBS, and fixation in formalin for 24 hours. The samples were then dehydrated in alcohol, cleared with xylene, and paraffin-embedded. Sections were cut at 4 μm, incubated at 58°C for 2 hours, dewaxed, and stained with hematoxylin for 5 minutes. After staining, the sections were dipped in 1% acid ethanol, rinsed, stained with eosin, dehydrated, cleared, and mounted with neutral resin. All reagents were purchased from ZSGB-BIO (Beijing, China). The pathological scoring standards of H&E include categories such as goblet cells, crypt abscess, mucosal destruction, muscle thickening, and inflammatory cell infiltration.[15]

AB-PAS staining was conducted according to the manufacturer's instructions, followed by dehydration via the H&E protocol. Images were captured via a K-viewer (Jiang Feng Company, China).

Total RNA Extraction and qPCR Analysis

Total RNA extraction and reverse transcription were performed as described previously.[16] The primer sequences were designed and provided by Shanghai Sangon Biotech Co., Ltd. Relative expression levels of genes (mRNA) were calculated using the $2^{\wedge(-\Delta\Delta Ct)}$ method. The primer sequences used for qPCR are shown in Table 2.

Western Blot Analysis

Lysed tissues and cells in RIPA buffer supplemented with PMSF (Biyuntian, Hangzhou, China) were separated via SDS–PAGE, subjected to PVDF transfer, and blocked with 5% milk. The samples were then incubated with antibodies overnight at 4°C, followed by secondary antibody treatment for 1 hour. Finally, the membranes were developed with enhanced chemiluminescence (ECL) (Biosharp, Hefei, China) for grayscale analysis via ImageJ (ImageJ Software Inc., USA). The dilution ratios of the antibodies used were as follows: HSP90AA1 (Santacruz, sc-515081, USA, 1:1000), p38 alpha/MAPK14 (MCE, HY-P80996, 1:1000), ZO-1 (Proteintech, 21773-1-AP, 1:5000), Occludin (Santacruz, sc-133256, 1:100), Claudin-1 (Abcam, ab307692, 1:1000), JAM-A (Proteintech, 16183-1-AP, 1:1000), goat anti-rabbit IgG (H+L)-HRP conjugate (Bio-Rad, 1706515, USA, 1:1000), and goat anti-mouse IgG (H+L)-HRP conjugate (Bio-Rad, 1706516, USA, 1:1000).

Table 2 Primers for qRT-PCR

Gene	Primer
β-actin (human)	Forward 5'-CTCCATCCTGGCCTCGCTGT-3' Reverse 5'-GCTGTCACCTTCACCGTTCC-3'
Mitogen-activated protein kinase 14 (MAPK14) (human)	Forward 5'-TGCTGGAGAAGATGCTTGTATTGG-3' Reverse 5'-GGTTCATCAGGATCGTGGTAC-3'
Heat shock protein 90 alpha family class A member 1 (HSP90AA1) (human)	Forward 5'-ATCCACCACTCTACTCTGTCTCTG-3' Reverse 5'-GCACCTTGGCTCTGTCTGAAG-3'
Occludin (human)	Forward 5'-AACTTCGCCTGTGGATGACTTCAG-3' Reverse 5'-TTTGACCTTCCTGCTCTTCCCTTTG-3'
Zonula Occludens-1 (ZO-1) (human)	Forward 5'-GCATGATGATCGTCTGTCCTACCTG-3' Reverse 5'-CCGCCTTCTGTGTCTGTGTCTTC-3'
Claudin-1 (human)	Forward 5'-GGTCTTGCCGCCTTGGTAGC-3' Reverse 5'-AGGACAGGAACAGGAGAGCAGTG-3'
Junctional Adhesion Molecule-A (JAM-A) (human)	Forward 5'-GCCTCTTCATATTGGCGATCC-3' Reverse 5'-CCGAGTAGGCACAGGACAACTT-3'
GAPDH (mouse)	Forward 5'-AAATGGTGAAGGTCGGTGTGAAC-3' Reverse 5'-CAACAATCTCCACTTTGCCACTG-3'
MAPK14 (mouse)	Forward 5'-TGTGATTGGTCTGTTGGATGTGTTCG-3' Reverse 5'-TGGCACTTCACGATGTTGTTCAG-3'
HSP90AA1 (mouse)	Forward 5'-ATCACGAAGCATAACGACGATGAG-3' Reverse 5'-TAACCTTTGTTCCACGACCCATTG-3'
Occludin (mouse)	Forward 5'-CCTCTGACCTTGAGTGTGGATGAC-3' Reverse 5'-TCCTCTTGCCCTTTCCTGCTTTC-3'
ZO-1 (mouse)	Forward 5'-ACCCGAAACTGATGCTGTGGATAG-3' Reverse 5'-GCTGGCTGGCTGTACTGTGAG-3'
Claudin-1 (mouse)	Forward 5'-GTGTCCTACTTTCCTGCTCCTGTC-3' Reverse 5'-AGAAGGTGTTGGCTTGGGATAAGG-3'
JAM-A (mouse)	Forward 5'-ACCTACTCTGGCTTCTCCTCTCC-3' Reverse 5'–GAAGGTGACTCGGTCCGCATAG3'

Immunofluorescence Assay

The sections were dewaxed, dehydrated, and subjected to antigen retrieval with Tris-EDTA (BL617A, Biosharp, China). The samples were blocked with 5% BSA, incubated with primary antibodies overnight at 4°C, washed, and then incubated with fluorescent secondary antibodies for 1 hour in the dark. Nuclei were stained with DAPI, mounted with an anti-quenching agent, and imaged with a fluorescence microscope. Images can then be captured via a fluorescence inverted microscope. The dilution ratios of the antibodies used were as follows: HSP90AA1 (Santacruz, sc-515081, 1:100), p38 alpha/MAPK14 (MCE, HY-P80996, 1:50), ZO-1 (Abcam, ab276131, 1:500), Occludin (Santacruz, sc-133256, 1:100), Claudin-1 (Abcam, ab307692, 1:50), JAM-A ((Santacruz, sc-53623, 1:100), TNF-α (Santacruz, sc-52746, 1:100), goat anti-mouse IgG H&L (Alexa Fluor® 594) (Abcam, 1:1000), and goat anti-rabbit IgG H&L (Alexa Fluor® 488) (Abcam, 1:1000) antibodies.

Statistical Analysis

Data analysis was conducted with GraphPad Prism 9.2, and the results are presented as the means ± SD. One-way ANOVA and Tukey's test were used to assess group differences, with $P < 0.05$ indicating significance, *$P< 0.05$, **$P<0.01$, ***$P<0.001$. Unless otherwise stated, all experiments were repeated at least three times.

Results

Network-Based Screening and Modular Profiling of BBR Targets for CD Therapy

The chemical structure of BBR was shown in Figure 1A. A total of 107 potential targets were intersected (Figure 1B). These targets were stratified into six functional modules, with core module 1 displaying the highest network complexity, containing 22 nodes and 204 edges. Key hub genes within this module include MMP9, HSP90AA1, GSK3B, ESR1, CASP3, IGF1R, CCL5, AR, ANXA5, ALB, IGF1, EGFR, KDR, MMP2, PTPN1, MAPK14, PPARA, IL2, MAP2K1, STAT1, PPARG, and SRC (Figure 1C). GO analysis demonstrated significant enrichment in biological processes including response to peptides, membrane microdomain organization, and protein serine/threonine/tyrosine kinase activity (Figure 1D). KEGG analysis revealed predominant association with the MAPK signaling cascade (Figure 1E).

MR to Screen Exposed Genes for CD Pathogenesis

In investigating the etiological risk factors for CD, MR employs genetic variation as an instrumental variable to infer the causal relationship between exposure and outcome. The IVW method was used for analysis. This result was consistent

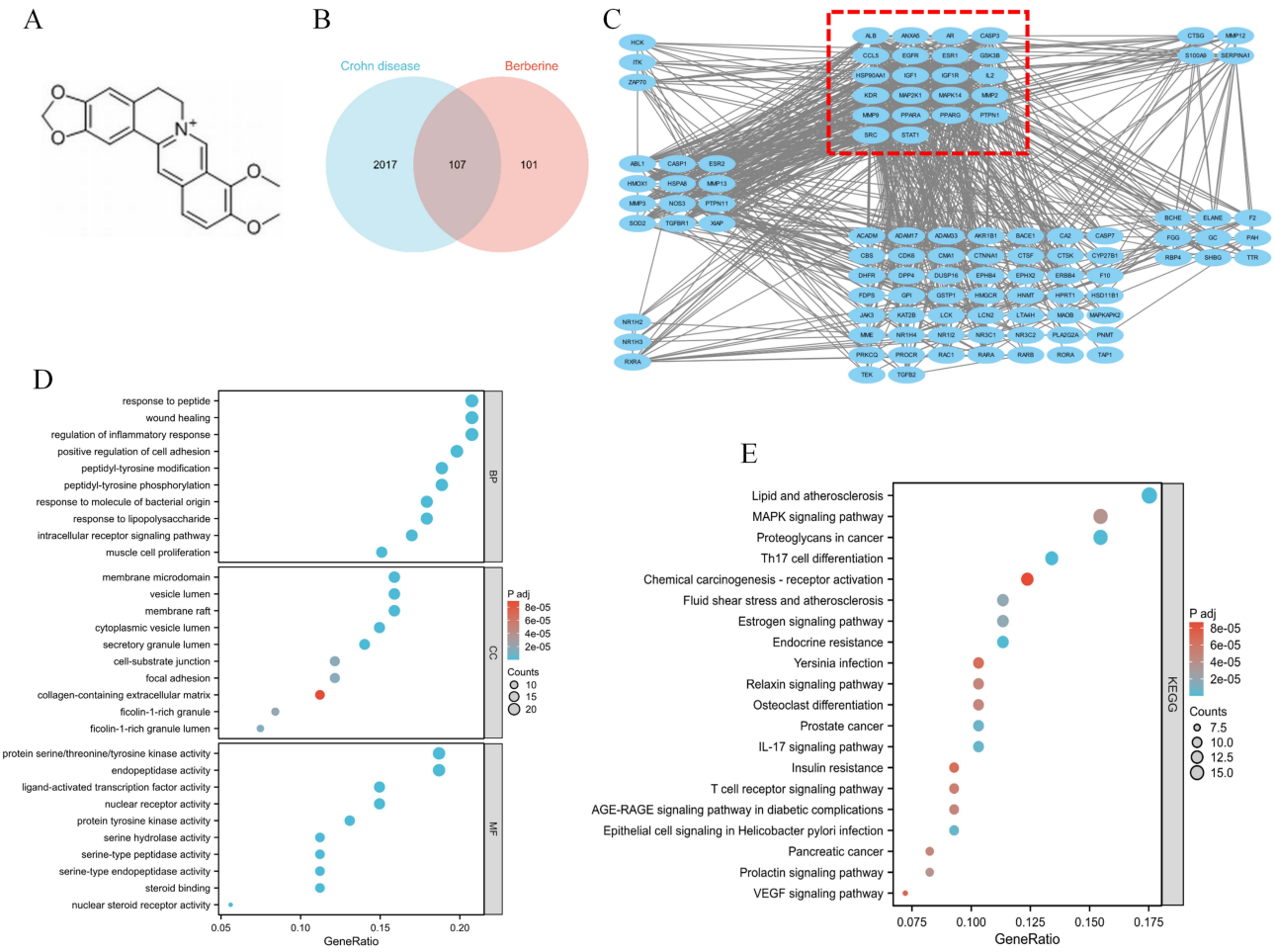

Figure 1 BBR targets and pathways in CD therapeutics. (**A**) The chemical structure of BBR. (**B**) Venn diagram of BBR targets in CD treatment. (**C**) PPI network and Core module analysis identifies key BBR targets in CD treatment, with core module 1 marked in red. (**D**) GO analyses of core module 1. (**E**) KEGG analyses of core module 1.

with $P<0.05$, and the β values were in the same direction. The gene was considered to have a causal relationship with the disease. The F statistic for each SNP was greater than 10, indicating less weak instrument bias (Table S1). Our findings indicate that MAPK14 and HSP90AA1 may serve as exposure factors in the pathogenesis of CD (Figure 2).

Protein	method	nSNP	Pval	OR(95%CI)
ANXA5	MR Egger	40	0.804390376	0.99(0.92 to 1.07)
ANXA5	Weighted median	40	0.435623539	0.98(0.93 to 1.03)
ANXA5	Inverse variance weighted	40	0.055349017	0.96(0.92 to 1.00)
ANXA5	Simple mode	40	0.157377195	0.94(0.87 to 1.02)
ANXA5	Weighted mode	40	0.144977568	0.96(0.91 to 1.01)
CASP3	*MR Egger*	*23*	*0.042227958*	*1.17(1.02 to 1.35)*
CASP3	Weighted median	23	0.111032927	1.08(0.98 to 1.18)
CASP3	Inverse variance weighted	23	0.087810455	1.08(0.99 to 1.17)
CASP3	Simple mode	23	0.722422926	1.03(0.88 to 1.21)
CASP3	Weighted mode	23	0.343864295	1.05(0.95 to 1.15)
CCL5	MR Egger	9	0.525269076	1.16(0.76 to 1.77)
CCL5	Weighted median	9	0.781899563	0.97(0.79 to 1.19)
CCL5	Inverse variance weighted	9	0.146475248	0.89(0.76 to 1.04)
CCL5	Simple mode	9	0.966749024	0.99(0.73 to 1.34)
CCL5	Weighted mode	9	0.964292842	1.01(0.77 to 1.31)
ESR1	MR Egger	8	0.567528953	0.81(0.40 to 1.62)
ESR1	Weighted median	8	0.992289753	1.00(0.74 to 1.34)
ESR1	Inverse variance weighted	8	0.930806436	1.01(0.80 to 1.27)
ESR1	Simple mode	8	0.780775943	1.07(0.66 to 1.75)
ESR1	Weighted mode	8	0.964713257	0.99(0.71 to 1.39)
GSK3B	MR Egger	44	0.777535790	1.02(0.90 to 1.16)
GSK3B	*Weighted median*	*44*	*0.020422381*	*0.91(0.84 to 0.99)*
GSK3B	*Inverse variance weighted*	*44*	*0.014070296*	*0.93(0.88 to 0.99)*
GSK3B	Simple mode	44	0.302984483	1.08(0.94 to 1.24)
GSK3B	Weighted mode	44	0.073326057	0.92(0.85 to 1.01)
HSP90AA1	MR Egger	19	0.681800463	0.95(0.74 to 1.22)
HSP90AA1	*Weighted median*	*19*	*0.015694801*	*0.84(0.73 to 0.97)*
HSP90AA1	*Inverse variance weighted*	*19*	*0.001349795*	*0.85(0.77 to 0.94)*
HSP90AA1	*Simple mode*	*19*	*0.026956309*	*0.79(0.65 to 0.96)*
HSP90AA1	*Weighted mode*	*19*	*0.018354814*	*0.82(0.70 to 0.95)*
IGF1R	MR Egger	39	0.223642271	0.85(0.65 to 1.10)
IGF1R	Weighted median	39	0.776880510	1.02(0.88 to 1.20)
IGF1R	Inverse variance weighted	39	0.536370858	0.97(0.87 to 1.07)
IGF1R	Simple mode	39	0.881413171	1.02(0.79 to 1.31)
IGF1R	Weighted mode	39	0.953950363	0.99(0.82 to 1.21)
MAP2K1	MR Egger	17	0.674410910	0.92(0.61 to 1.37)
MAP2K1	Weighted median	17	0.224246441	1.13(0.93 to 1.38)
MAP2K1	Inverse variance weighted	17	0.165012101	1.11(0.96 to 1.29)
MAP2K1	Simple mode	17	0.812823949	1.04(0.76 to 1.42)
MAP2K1	Weighted mode	17	0.352270436	1.12(0.89 to 1.40)
MAPK14	MR Egger	19	0.868359420	1.02(0.78 to 1.35)
MAPK14	Weighted median	19	0.073088559	1.13(0.99 to 1.28)
MAPK14	*Inverse variance weighted*	*19*	*0.010076258*	*1.14(1.03 to 1.25)*
MAPK14	Simple mode	19	0.098120188	1.17(0.98 to 1.40)
MAPK14	Weighted mode	19	0.163340602	1.13(0.96 to 1.33)
PPARA	MR Egger	6	0.530415664	1.35(0.58 to 3.15)
PPARA	Weighted median	6	0.368419173	0.83(0.56 to 1.24)
PPARA	Inverse variance weighted	6	0.886794283	0.97(0.69 to 1.38)
PPARA	Simple mode	6	0.386743865	0.78(0.47 to 1.30)
PPARA	Weighted mode	6	0.381523348	0.79(0.49 to 1.28)
PPARG	MR Egger	38	0.659033829	1.04(0.87 to 1.25)
PPARG	Weighted median	38	0.317789203	1.06(0.95 to 1.17)
PPARG	Inverse variance weighted	38	0.892103568	0.99(0.92 to 1.07)
PPARG	Simple mode	38	0.497440851	1.06(0.90 to 1.26)
PPARG	Weighted mode	38	0.268536116	1.07(0.95 to 1.21)
PTPN1	*MR Egger*	*16*	*0.030407256*	*0.80(0.67 to 0.96)*
PTPN1	Weighted median	16	0.217959412	0.92(0.79 to 1.05)
PTPN1	Inverse variance weighted	16	0.911732197	0.99(0.86 to 1.15)
PTPN1	Simple mode	16	0.636809401	0.94(0.73 to 1.21)
PTPN1	Weighted mode	16	0.116971192	0.89(0.77 to 1.02)
SRC	MR Egger	4	0.913451227	0.95(0.42 to 2.15)
SRC	Weighted median	4	0.113924125	0.70(0.45 to 1.09)
SRC	Inverse variance weighted	4	0.098058804	0.72(0.50 to 1.06)
SRC	Simple mode	4	0.268388444	0.68(0.39 to 1.19)
SRC	Weighted mode	4	0.283414160	0.69(0.39 to 1.21)
STAT1	MR Egger	3	0.620167609	2.36(0.20 to 28.27)
STAT1	Weighted median	3	0.333591308	0.77(0.45 to 1.31)
STAT1	Inverse variance weighted	3	0.320702038	0.79(0.49 to 1.26)
STAT1	Simple mode	3	0.310324072	0.63(0.32 to 1.24)
STAT1	Weighted mode	3	0.351612015	0.67(0.35 to 1.29)

P<0.05 was considered statistically significant

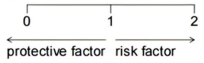

Figure 2 MR indicates specific genes that are causally associated with CD. Genes reaching statistical significance ($P < 0.05$) are highlighted in red.

https://doi.org/10.2147/PGPM.S547308

Table 3 Docking Scores

Protein	Chem ID	Name	Docking Score
HSP90AA1	2353	Berberine	−3.425
MAPK14	2353	Berberine	−6.058

Molecular Docking and Molecular Dynamics Simulations of BBR Interactions with MAPK14 and HSP90AA1

The molecular docking data indicate that BBR has a strong binding affinity for both MAPK14 and HSP90AA1 (detailed docking scores are shown in Table 3), with interactions occurring via hydrogen bonds, carbon–hydrogen bonds, and other interactions. Additionally, molecular dynamics simulations revealed that BBR maintains stable interactions with MAPK14 and HSP90AA1 (Figure 3A and B).

To verify the binding stability and mode of BBR to the receptor proteins MAPK14 and HSP90AA1, we assessed the stability of the system and the calculated compounds during molecular dynamics simulations by calculating the RMSD and RMSF of the amino acid backbone atoms of the receptor protein complex. The results indicate that BBR binds to both

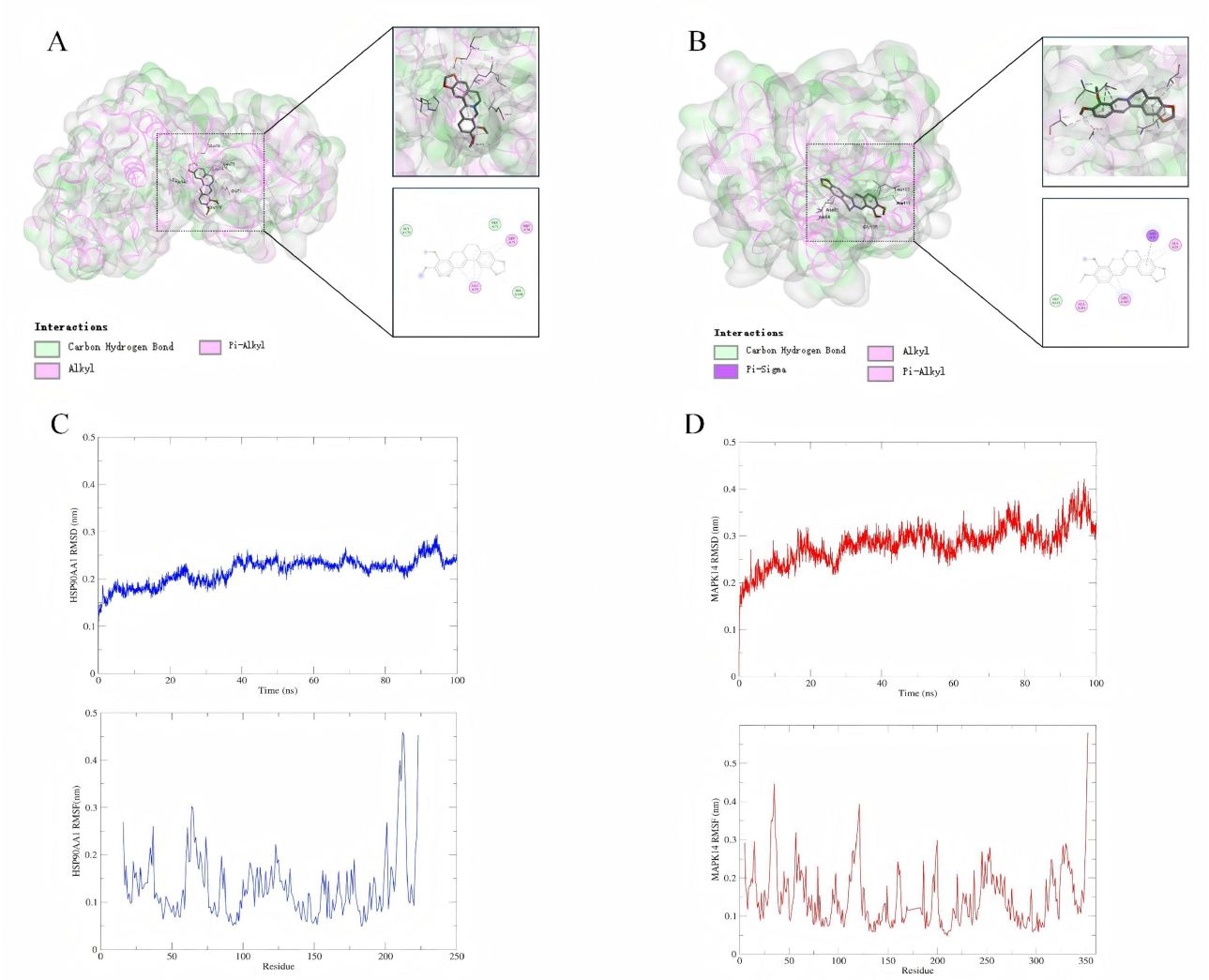

Figure 3 Computational analysis of BBR, MAPK14 and HSP90AA1. (**A**) Molecular docking of HSP90AA1 and BBR. (**B**) Molecular docking of MAPK14 and BBR. (**C**) RMSD and RMSF analysis of HSP90AA1 and BBR. (**D**) RMSD and RMSF analysis of MAPK14 and BBR.

MAPK14 and HSP90AA1, resulting in low RMSD and RMSF values, which suggests that their combination is stable (Figure 3C and D). From an molecular dynamics perspective, BBR can stably bind to the MAPK14 and HSP90AA1 proteins.

BBR Downregulates HSP90AA1 and MAPK14 in Caco-2 Cells

CCK-8 assays demonstrated dose-dependent suppression of Caco-2 cells proliferation by BBR. Notably, concentrations of 5, 10, and 20 μM exerted no cytotoxic effects on cell viability during 24-hour exposure (Figure 4A). qPCR and WB analyses confirmed BBR's ability to attenuate LPS-induced upregulation of HSP90AA1 and MAPK14 expression (Figure 4B and C). Concurrently, BBR suppressed LPS-stimulated TNF-α secretion in cell supernatants (Figure 4D).

Effect of BBR on ZO-1, Occludin, Claudin-1, and JAM-A Expression in Caco-2 Cells

qPCR and WB analyses demonstrated that LPS significantly downregulated the expression of ZO-1, Occludin, Claudin-1, and JAM-A in Caco-2 cells. Conversely, BBR treatment dose-dependently upregulated these TJ proteins within defined concentration thresholds (Figure 5A and B). Immunofluorescence quantification confirmed LPS-induced attenuation of ZO-1, Occludin, Claudin-1, and JAM-A signals, which were rescued by BBR exposure (Figure 5C and D).

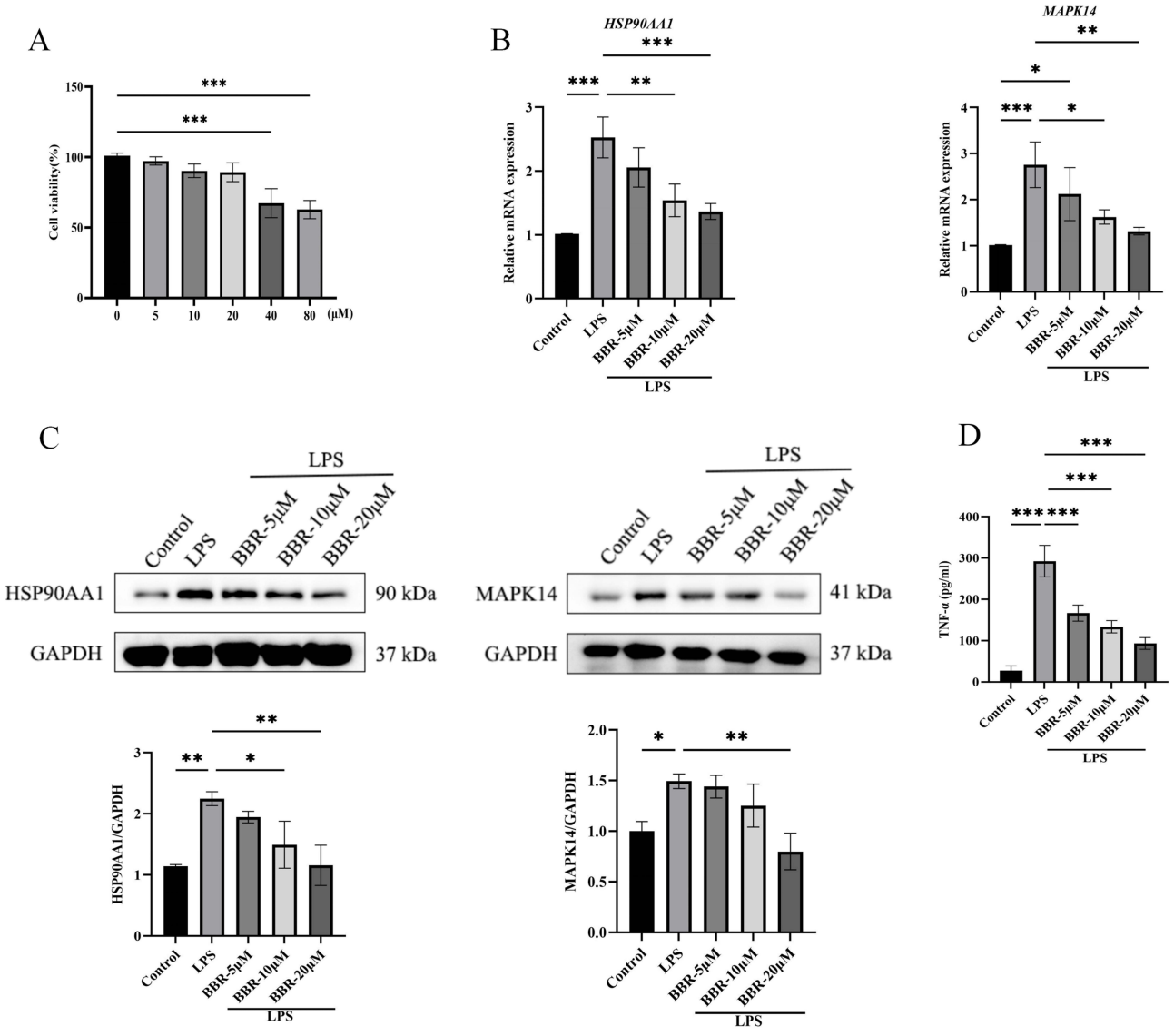

Figure 4 BBR attenuates LPS-induced inflammation in Caco-2 cells. (**A**) BBR-induced cytotoxicity quantified by CCK-8 assay following 24 hours exposure. (**B**) qPCR analysis of HSP90AA1 and MAPK14 expression post-LPS (1μg/mL) and BBR (5, 10, 20 μM) treatment. (**C**) WB analysis of HSP90AA1 and MAPK14. (**D**) TNF-α concentration in cell culture supernatant measured by ELISA. **P*<0.05, ***P*<0.01, ****P*<0.001.

https://doi.org/10.2147/PGPM.S547308

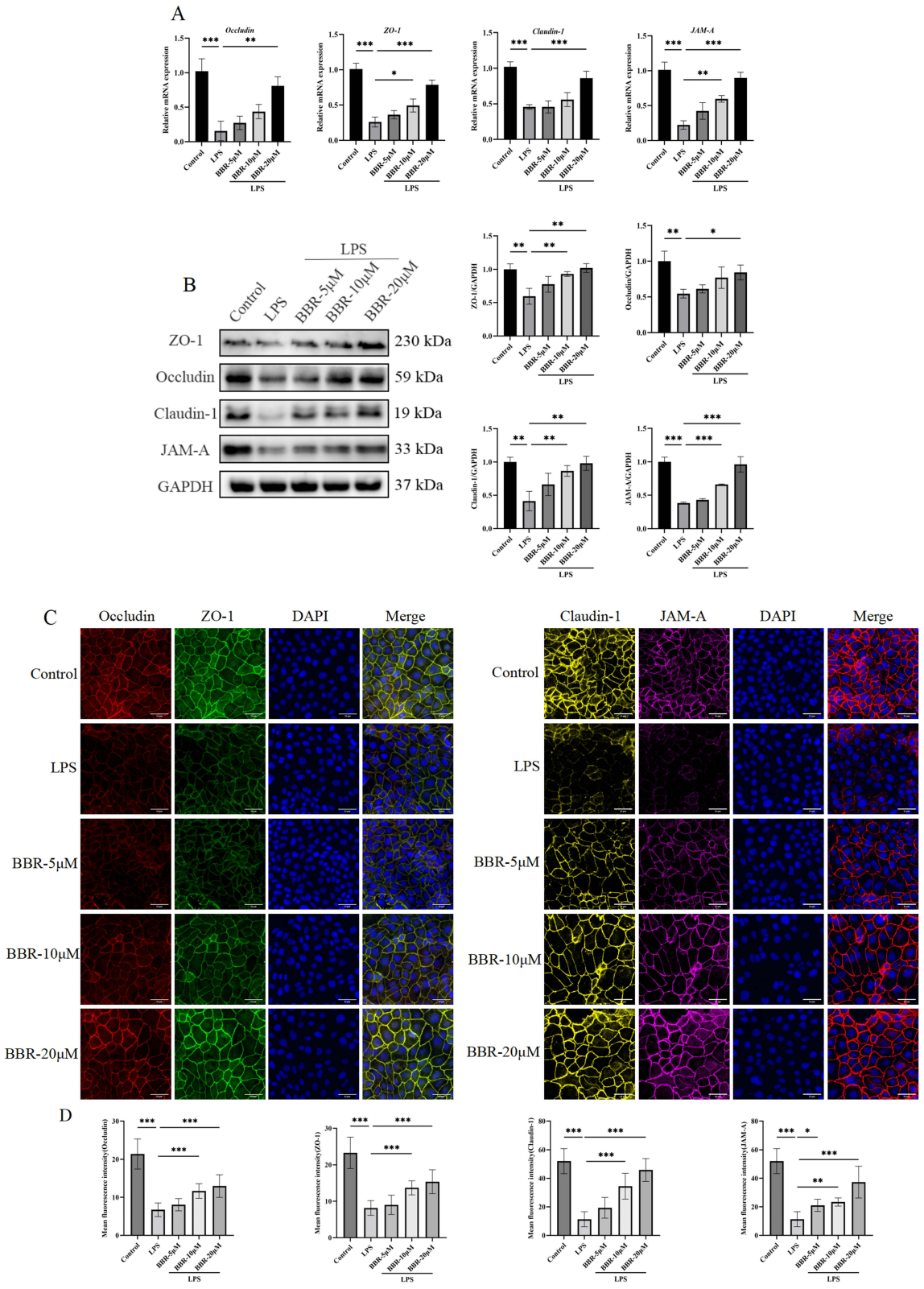

Figure 5 BBR attenuates LPS-induced barrier dysfunction in Caco-2 intestinal epithelium. (**A**) qPCR analysis of ZO-1, Occludin, Claudin-1, and JAM-A mRNA expression. (**B**) WB analysis of ZO-1, Occludin, Claudin-1, and JAM-A protein expression. (**C**) Representative fluorescence images of ZO-1, Occludin, Claudin-1, and JAM-A. (**D**) Analysis of fluorescence intensity for ZO-1, Occludin, Claudin-1, and JAM-A. **P*<0.05, ***P*<0.01, ****P*<0.001.

HSP90AA1 and MAPK14 Regulate Intestinal Mucosal Barrier Integrity

Experimental analyses revealed that both 17-AAG (HSP90AA1 inhibitor) and SB203580 (MAPK14 inhibitor) markedly upregulated mRNA levels of ZO-1, Occludin, Claudin-1, and JAM-A in Caco-2 cells (Figure 6A). Concurrently, these compounds enhanced protein expression (Figure 6B) and fluorescence intensity (Figure 6C and D) of the aforementioned TJs, with no significant difference in efficacy observed between the two treatments. These findings highlight the therapeutic potential of dual HSP90AA1 and MAPK14 inhibition in restoring intestinal mucosal barrier homeostasis under inflammatory conditions.

BBR Attenuates DSS-Induced Colonic Inflammatory Pathogenesis in Murine Models

To investigate the impact of BBR in vivo, we utilized DSS mice, a well-established model for CD-induced colitis.[14] The DSS exposure duration and BBR treatment doses applied in the colitis model are schematically summarized in Figure 7A. Our study revealed that BBR treatment effectively reduced weight loss (Figure 7B) and DAI score (Figure 7C) induced by DSS and attenuated colon shortening (Figure 7D and E). HE staining showed colonic crypt loss, inflammatory cell infiltration, and mucosal damage with elevated histopathological scores in DSS-treated mice; BBR treatment significantly reduced inflammation and scores (Figure 7F and G). Goblet cell numbers and mucin production decreased following DSS induction but markedly increased after BBR treatment (Figure 7H).

BBR restores colonic TJ proteins (ZO-1, Occludin, Claudin-1, JAM-A) in DSS-induced colitis (Figure 7I and J). HSP90AA1 and MAPK14 were highly expressed in DSS-treated mice but were reversed by BBR treatment (Figure 7K). Additionally, TNF-α levels were elevated in DSS-induced colitis tissues, yet BBR treatment significantly decreased TNF-α expression (Figure 7L). Collectively, our findings demonstrate that BBR treatment alleviates DSS-induced intestinal inflammation in murine models, restores intestinal mucosal barrier integrity, and exhibits dose-dependent therapeutic efficacy within a defined concentration range.

Discussion

In the pathogenesis of CD, destruction of the intestinal barrier leads to increased intestinal permeability, allowing pathogens and toxic substances to invade, triggering excessive immune responses and chronic inflammation.[17,18] Intestinal mucosal barrier repair is a critical stage in CD treatment,[19] although the underlying mechanisms remain unclear.

Our study identifies HSP90AA1 and MAPK14 as novel direct targets of BBR in the context of CD. A marked increase in MAPK14 and HSP90AA1 expression was observed in both LPS-stimulated cells and the colons of DSS-treated mice, which was accompanied by disruption of the intestinal mucosal barrier. Through pharmacological inhibition, we demonstrated that treatment with 17-AAG (HSP90AA1 inhibitor) or SB203580 (MAPK14 inhibitor) markedly restored the expression of TJ proteins, thereby functionally implicating both targets in the maintenance of intestinal barrier integrity. MAPK14 (p38α), a central component of the MAPK signaling pathway, transduces inflammatory and stress signals, regulating processes such as cell differentiation, apoptosis, and immune response.[20,21] Under inflammatory conditions, MAPK14 activation contributes significantly to intestinal epithelial damage by promoting apoptosis and downregulating key TJ proteins, thereby compromising mucosal barrier function.[22–25] Although the precise mechanisms require further investigation, existing evidence suggests that MAPK14 may regulate TJ proteins by phosphorylating key cytoskeletal or signaling components, thereby influencing their assembly and stability, particularly under inflammatory conditions.[23,25–27] HSP90AA1 (HSP90α), an inducible isoform of the heat shock protein 90 family, functions as a molecular chaperone that facilitates the stabilization and activation of numerous client proteins involved in signaling and stress response.[28,29] Its expression is upregulated during inflammation and cellular stress, and extracellular HSP90AA1 has been implicated in immune activation.[30] Clinically, elevated plasma levels of HSP90AA1 are observed in CD patients and correlate with disease severity, fatigue, and biomarkers such as CRP, highlighting its potential role as a pathogenic factor and biomarker in IBD.[30,31] Preclinical studies further suggest that HSP90 inhibition attenuates colitis partly through modulation of the MAPK pathway.[32] It is plausible that HSP90AA1 stabilizes MAPK14 or other inflammatory mediators, creating a pro-inflammatory loop that disrupts epithelial integrity. Although previous studies have reached conclusions similar to those presented herein, the specific role that BBR plays in this process remains unclear.

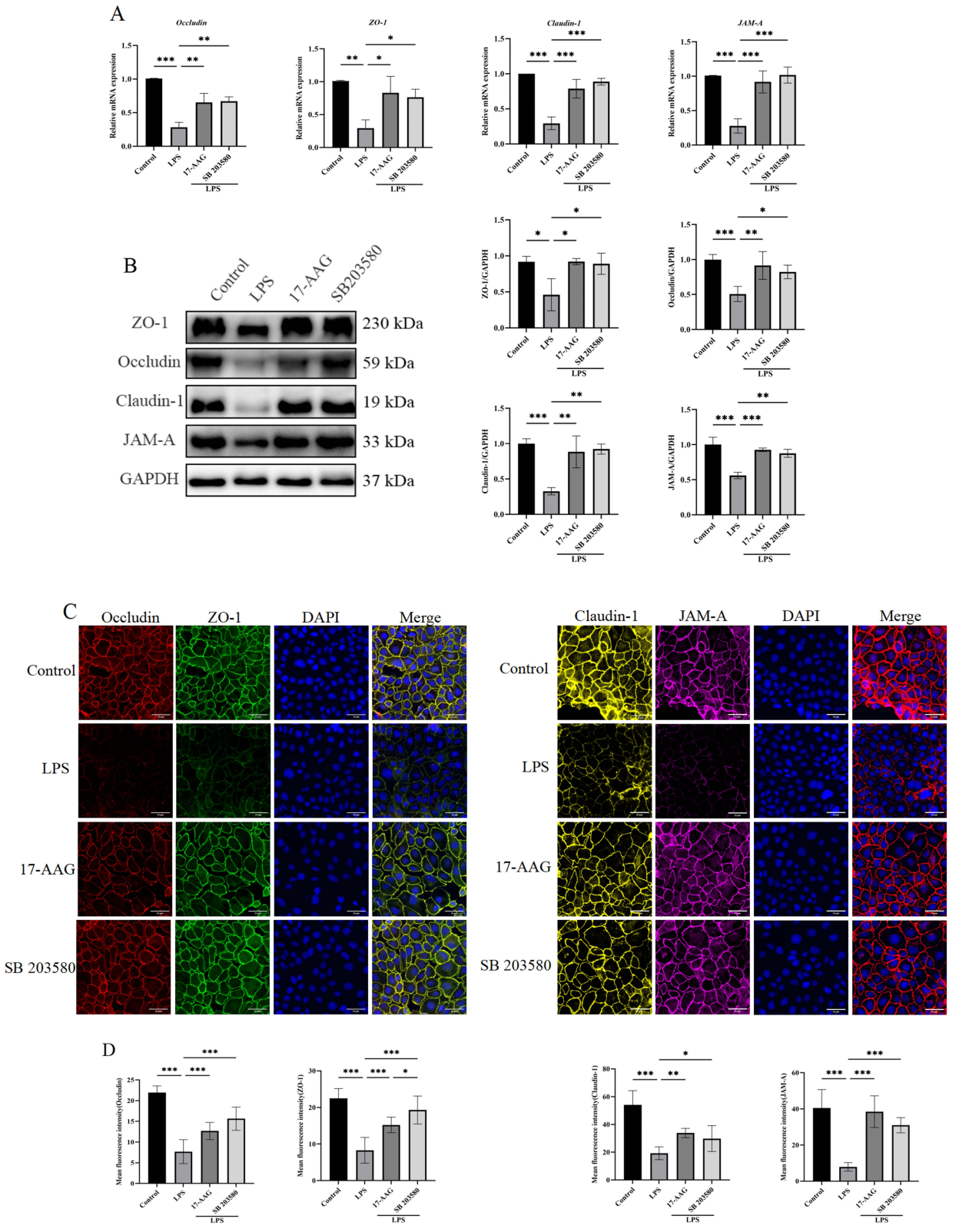

Figure 6 Modulatory effects of 17-AAG and SB203580 on LPS-induced intestinal epithelial barrier integrity in Caco-2 Cells. (**A**) qPCR analysis of ZO-1, Occludin, Claudin-1, and JAM-A mRNA expression after 17-AAG (0.5 μM) and SB203580 (20 nM) pretreatment for 1 hour and LPS (1μg/mL) exposure for 24 hours. (**B**) WB analysis of ZO-1, Occludin, Claudin-1, and JAM-A protein expression. (**C**) Representative fluorescence images of ZO-1, Occludin, Claudin-1, and JAM-A. (**D**) Analysis of fluorescence intensity for ZO-1, Occludin, Claudin-1, and JAM-A. **P*<0.05, ***P*<0.01, ****P*<0.001.

We demonstrate through integrated computational and experimental approaches that BBR binds stably to both HSP90AA1 and MAPK14, downregulates their expression, and thereby attenuates inflammation and restores TJ protein expression. Specifically, we show that BBR treatment counteracts LPS-induced upregulation of HSP90AA1 and MAPK14 in Caco-2 cells, reduces TNF-α secretion, and promotes the expression of ZO-1, Occludin, Claudin-1, and JAM-A. Importantly, in vivo results establish the therapeutic efficacy and dose-dependence of BBR in DSS-induced colitis. BBR treatment not only alleviated weight loss, disease activity, and colon shortening but also directly reduced HSP90AA1/MAPK14 expression and restored mucosal architecture and junctional protein levels—effects that were mechanistically consistent with our cellular findings. Numerous previous studies have demonstrated that BBR alleviates intestinal inflammation and restores the intestinal mucosal barrier through inhibition of multiple inflammatory pathways, including the MAPK signaling cascade.[33–35] Moreover, recent research has indicated that BBR potentially serves as a novel HSP90 inhibitor and exhibits a synergistic effect with the established Hsp90 inhibitor 17-AAG.[36]

While our integrated approach provides compelling evidence for the mechanism of BBR, this study has limitations. The primary one is the lack of validation in human primary cells, patient-derived organoids, or biopsy specimens.

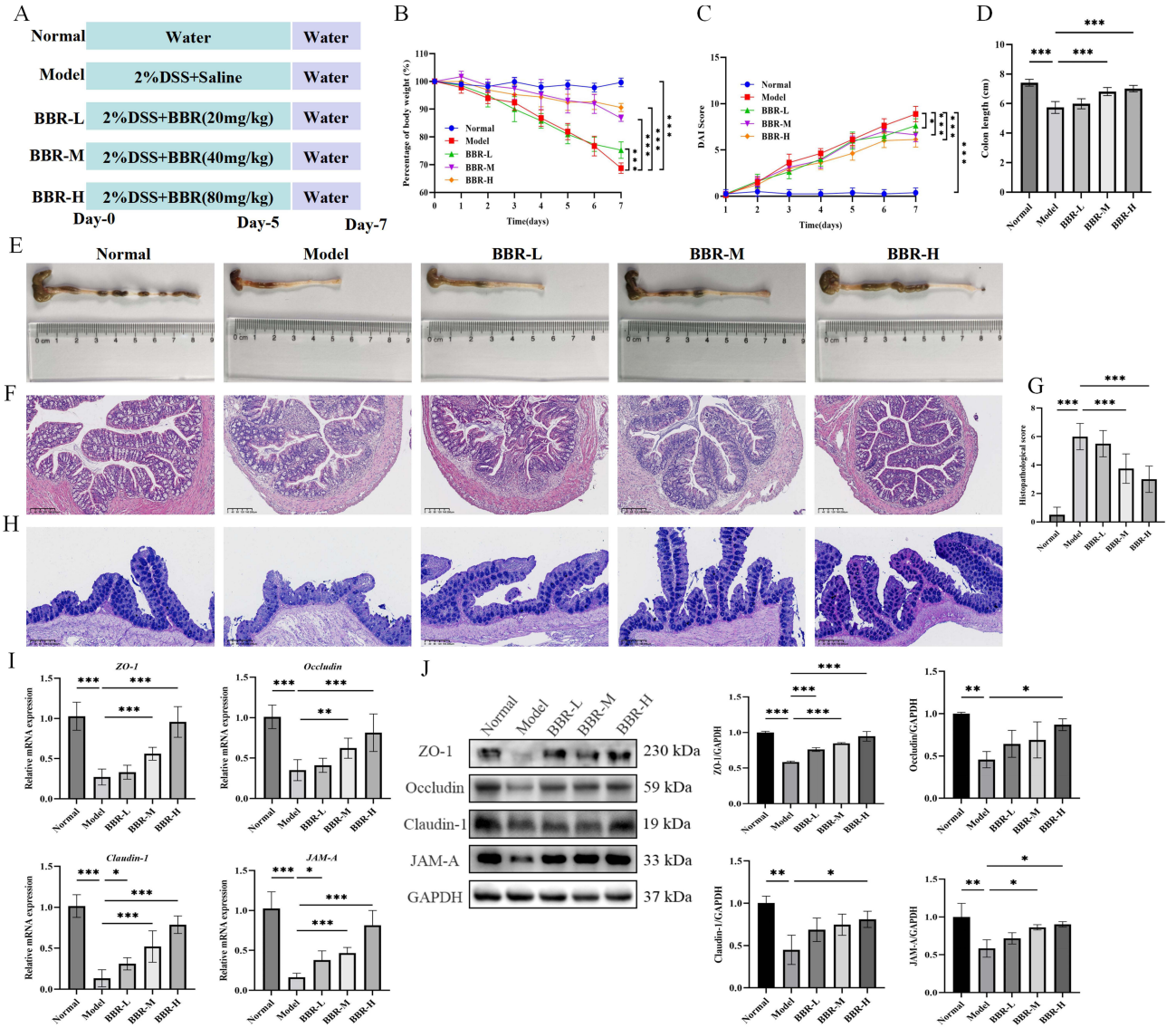

Figure 7 Continued.

https://doi.org/10.2147/PGPM.S547308

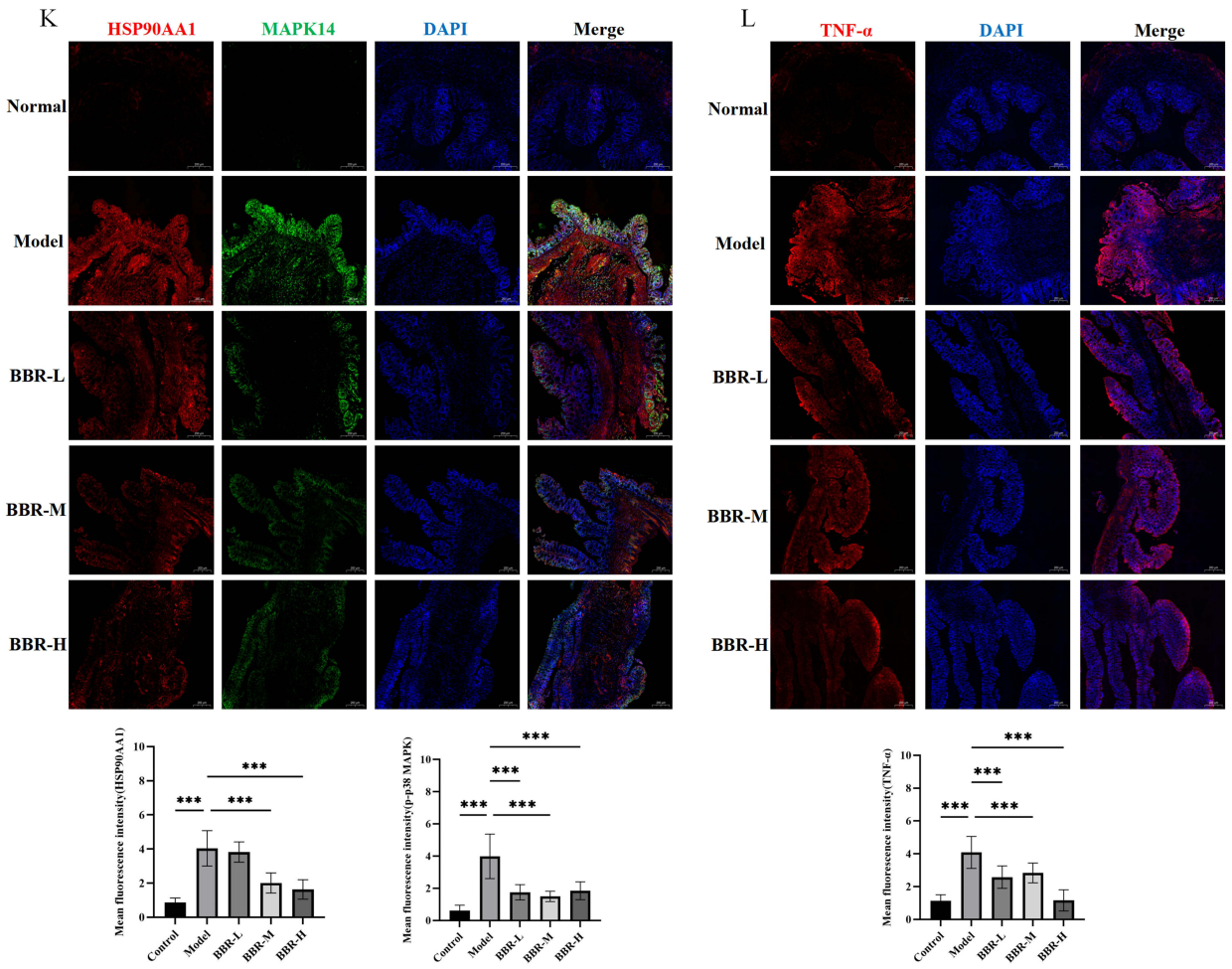

Figure 7 BBR attenuates DSS-induced murine colitis, n=8. (**A**) Schematic of BBR treatment in DSS model. (**B**) Daily weight change percentage. (**C**) DAI scores over 7 days. (**D**) Measurement of colonic length. (**E**) Representative images of colons. (**F**) Representative HE staining of colon tissues. (**G**) Statistical analysis of histological scores from HE staining. (**H**) AB-PAS staining. (**I**) qPCR analysis of ZO-1, Occludin, Claudin-1, and JAM-A mRNA expression. (**J**) WB analysis of ZO-1, Occludin, Claudin-1, and JAM-A protein expression. (**K**) Immunofluorescence analysis and quantitative fluorescence intensity profiling of HSP90AA1 and MAPK14 in colonic tissues, scale bar=200μm. (**L**) Immunofluorescence analysis and quantitative fluorescence intensity profiling of TNF-α in colonic tissues, scale bar=200 μm. **P*<0.05, ***P*<0.01, ****P*<0.001.

Although our MR analysis provides genetic evidence from human GWAS data, direct experimental confirmation in human tissue models is a crucial next step to fully establish clinical translatability. Future research will prioritize validating these findings in human-derived systems to bridge the gap between our preclinical findings and clinical application.

Conclusion

In conclusion, our study delved into the potential targets of BBR, providing evidence for its anti-inflammatory and immunoprotective properties. These findings may serve as a foundation for further research on the use of BBR as an alternative treatment approach for CD.

Abbreviations

ANOVA, one-way analysis of variance; BBR, berberine; CD, Crohn's disease; CRP, C-reactive protein; DSS, dextran sulfate sodium; DAI, disease activity index; ELISA, enzyme-linked immunosorbent assay; GO, Gene Ontology; HSP, heat shock protein; HSP90AA1, heat shock protein 90 alpha family member 1; IBD, inflammatory bowel disease; IVW,

inverse variance weighting; KEGG, Kyoto Encyclopedia of Genes and Genomes; MR, Mendelian randomization; MAPK14, mitogen-activated protein kinase 14; NCBI, National Center for Biotechnology Information; RMSD, root-mean-square deviation; RMSF, root-mean-square fluctuation; SD, standard deviation; STR, short tandem repeat; TNBS, 2,4,6-trinitrobenzenesulfonic acid; TNF-α, tumor necrosis factor alpha; TJ, tight junction.

Acknowledgments

This study solely relied on public, anonymized database data and did not involve any primary data collection from human or animal subjects, thus qualifying for exemption according to standard institutional and international guidelines. This study is exempt from ethical approval in accordance with national legislation, under items 1 and 2 of Article 32 of the "Measures for Ethical Review of Life Science and Medical Research Involving Human Subjects dates February 18, 2023, China".

We gratefully acknowledge the following public databases for providing valuable resources: PubChem (compound structure), PharmMapper (target prediction), UniProt (gene annotation), GeneCards (disease targets), STRING (protein interactions), FinnGen Consortium (GWAS data), and RCSB PDB (protein structures). Their contributions were essential to this study.

Author Contributions

All authors made a significant contribution to the work reported, whether that is in the conception, study design, execution, acquisition of data, analysis and interpretation, or in all these areas; took part in drafting, revising or critically reviewing the article; gave final approval of the version to be published; have agreed on the journal to which the article has been submitted; and agree to be accountable for all aspects of the work.

Funding

This work was supported by the Youth Foundation of the Hangzhou Red Cross Hospital (No.HHQN2024001), the China Postdoctoral Science Foundation under Grant Number (2024MD753922), and the Guangxi Youth Qihuang Scholar Training Program (GXQH202419).

Disclosure

Danya Zhao, Yang Zhai, and Chen Chen are co-first authors for this study. This authors report no conflicts of interest in this work.

References

1. Dolinger M, Torres J, Vermeire S. Crohn's disease. *Lancet*. 2024;403(10432):1177–1191. doi:10.1016/S0140-6736(23)02586-2
2. Torres J, Mehandru S, Colombel JF, Peyrin-Biroulet L. Crohn's disease. *Lancet*. 2017;389(10080):1741–1755. doi:10.1016/S0140-6736(16)31711-1
3. Tachibana K, Bai L, Sugimura S, et al. Heterogenous gene expression of bicellular and tricellular tight junction-sealing components in the human intestinal tract. *Biol Pharm Bull*. 2024;47(6):1209–1217. doi:10.1248/bpb.b23-00927
4. Jian Y, Zhang D, Liu M, Wang Y, Xu ZX. The impact of gut microbiota on radiation-induced enteritis. *Front Cell Infect Microbiol*. 2021;11:586392. doi:10.3389/fcimb.2021.586392
5. Li J, Liu X, Wu Y, Ji W, Tian Q, Li S. Aerobic exercise improves intestinal mucosal barrier dysfunction through TLR4/MyD88/NF-κB signaling pathway in diabetic rats. *Biochem Biophys Res Commun*. 2022;634:75–82. doi:10.1016/j.bbrc.2022.09.075
6. Hartmann C, Schwietzer YA, Otani T, Furuse M, Ebnet K. Physiological functions of junctional adhesion molecules (JAMs) in tight junctions. *Biochim Biophys Acta Biomembr*. 2020;1862(9):183299. doi:10.1016/j.bbamem.2020.183299
7. Guo H, Guo H, Xie Y, et al. Mo3Se4 nanoparticle with ROS scavenging and multi-enzyme activity for the treatment of DSS-induced colitis in mice. *Redox Biol*. 2022;56:102441. doi:10.1016/j.redox.2022.102441
8. Li Y, Ren G, Wang YX, et al. Bioactivities of berberine metabolites after transformation through CYP450 isoenzymes. *J Transl Med*. 2011;9:62. doi:10.1186/1479-5876-9-62
9. Dong Y, Fan H, Zhang Z, et al. Berberine ameliorates DSS-induced intestinal mucosal barrier dysfunction through microbiota-dependence and Wnt/β-catenin pathway. *Int J Biol Sci*. 2022;18(4):1381–1397. doi:10.7150/ijbs.65476
10. Wang X, Shen Y, Wang S, et al. PharmMapper 2017 update: a web server for potential drug target identification with a comprehensive target pharmacophore database. *Nucleic Acids Res*. 2017;45(W1):W356–W360. doi:10.1093/nar/gkx374
11. Pronk S, Páll S, Schulz R, et al. GROMACS 4.5: a high-throughput and highly parallel open source molecular simulation toolkit. *Bioinformatics*. 2013;29(7):845–854. doi:10.1093/bioinformatics/btt055
12. Van Der Spoel D, Lindahl E, Hess B, Groenhof G, Mark AE, Berendsen HJC. GROMACS: fast, flexible, and free. *J Comput Chem*. 2005;26(16):1701–1718. doi:10.1002/jcc.20291

13. Kagami L, Wilter A, Diaz A, Vranken W. The ACPYPE web server for small-molecule MD topology generation. *Bioinformatics*. 2023;39(6): btad350. doi:10.1093/bioinformatics/btad350
14. Wen W, Xu Y, Qian W, et al. PUFAs add fuel to Crohn's disease-associated AIEC-induced enteritis by exacerbating intestinal epithelial lipid peroxidation. *Gut Microbes*. 2023;15(2):2265578. doi:10.1080/19490976.2023.2265578
15. Sałaga M, Mokrowiecka A, Zakrzewski PK, et al. Experimental colitis in mice is attenuated by changes in the levels of endocannabinoid metabolites induced by selective inhibition of fatty acid amide hydrolase (FAAH). *J Crohns Colitis*. 2014;8(9):998–1009. doi:10.1016/j.crohns.2014.01.025
16. Zhao D, Qin D, Yin L, Yang Q. Integrated bioinformatics analysis and experimental verification of immune cell infiltration and the related core genes in ulcerative colitis. *Pharmgenomics Pers Med*. 2023;16:629–643. doi:10.2147/PGPM.S406644
17. Luissint AC, Parkos CA, Nusrat A. Inflammation and the intestinal barrier: leukocyte-epithelial cell interactions, cell junction remodeling, and mucosal repair. *Gastroenterology*. 2016;151(4):616–632. doi:10.1053/j.gastro.2016.07.008
18. Schirmer M, Garner A, Vlamakis H, Xavier RJ. Microbial genes and pathways in inflammatory bowel disease. *Nat Rev Microbiol*. 2019;17(8):497–511. doi:10.1038/s41579-019-0213-6
19. Huang S, Xie Z, Han J, et al. Protocadherin 20 maintains intestinal barrier function to protect against Crohn's disease by targeting ATF6. *Genome Biol*. 2023;24:159. doi:10.1186/s13059-023-02991-0
20. Park HB, Baek KH. E3 ligases and deubiquitinating enzymes regulating the MAPK signaling pathway in cancers. *Biochimica Et Biophysica Acta*. 2022;1877(3):188736. doi:10.1016/j.bbcan.2022.188736
21. Dahm K, Vijayarangakannan P, Wollscheid HP, Schild H, Rajalingam K. Atypical MAPKs in cancer. *FEBS J*. 2025;292(9):2173–2188. doi:10.1111/febs.17283
22. Xiong W, Huang J, Li X, et al. Icariin and its phosphorylated derivatives alleviate intestinal epithelial barrier disruption caused by enterotoxigenic Escherichia coli through modulate p38 MAPK in vivo and in vitro. *FASEB J*. 2020;34(1):1783–1801. doi:10.1096/fj.201902265R
23. Xue HH, Li JJ, Li SF, et al. Phillygenin attenuated colon inflammation and improved intestinal mucosal barrier in DSS-induced colitis mice via TLR4/Src mediated MAPK and NF-κB signaling pathways. *Int J Mol Sci*. 2023;24(3):2238. doi:10.3390/ijms24032238
24. Xiang DC, Yang JY, Xu YJ, et al. Protective effect of Andrographolide on 5-Fu induced intestinal mucositis by regulating p38 MAPK signaling pathway. *Life Sciences*. 2020;252:117612. doi:10.1016/j.lfs.2020.117612
25. Zhang Z, Zhang Q, Li F, Xin Y, Duan Z. Contributions of HO-1-dependent MAPK to regulating intestinal barrier disruption. *Biomol Ther*. 2021;29(2):175–183. doi:10.4062/biomolther.2020.112
26. Ran X, Li Y, Chen G, et al. Farrerol ameliorates TNBS-induced colonic inflammation by inhibiting ERK1/2, JNK1/2, and NF-κB signaling pathway. *Int J Mol Sci*. 2018;19(7):2037. doi:10.3390/ijms19072037
27. Yang M, Xu W, Yue C, et al. Adipose-derived stem cells promote the recovery of intestinal barrier function by inhibiting the p38 MAPK signaling pathway. *Eur J Histochem*. 2025;69(1):4158. doi:10.4081/ejh.2025.4158
28. Scalia F, Carini F, David S, et al. Inflammatory bowel diseases: an updated overview on the heat shock protein involvement. *Int J Mol Sci*. 2023;24(15):12129. doi:10.3390/ijms241512129
29. Shahana MV, Choudhary B. HSP90 and the cancer transcriptome: a comprehensive review of inhibitors and mechanistic insights. *Int J Clin Oncol*. 2025;30(7):1294–1308. doi:10.1007/s10147-025-02782-6
30. Prodromou C. Mechanisms of Hsp90 regulation. *Biochem J*. 2016;473(16):2439–2452. doi:10.1042/BCJ20160005
31. Grimstad T, Kvivik I, Kvaløy JT, Aabakken L, Omdal R. Heat shock protein 90 and inflammatory activity in newly onset Crohn's disease. *Scand J Gastroenterol*. 2018;53(12):1453–1458. doi:10.1080/00365521.2018.1533582
32. Yuan Y, Wu H, Shuai B, et al. Mechanism of HSP90 inhibitor in the treatment of DSS-induced colitis in mice by inhibiting MAPK pathway and synergistic effect of compound sophorae decoction. *Curr Pharm Des*. 2022;28(42):3456–3468. doi:10.2174/1381612829666221122113929
33. Zhu Z, Xueying L, Chunlin L, et al. Effect of berberine on LPS-induced expression of NF-κB/MAPK signalling pathway and related inflammatory cytokines in porcine intestinal epithelial cells. *Innate Immun*. 2020;26(7):627–634. doi:10.1177/1753425920930074
34. Zhao C, Wang Y, Yuan X, et al. Berberine inhibits lipopolysaccharide-induced expression of inflammatory cytokines by suppressing TLR4-mediated NF-κB and MAPK signaling pathways in rumen epithelial cells of Holstein calves. *J Dairy Res*. 2019;86(2):171–176. doi:10.1017/S0022029919000323
35. Tang M, Yuan D, Liao P. Berberine improves intestinal barrier function and reduces inflammation, immunosuppression, and oxidative stress by regulating the NF-κB/MAPK signaling pathway in deoxynivalenol-challenged piglets. *Environ Pollut*. 2021;289:117865. doi:10.1016/j.envpol.2021.117865
36. Li G, Zhang C, Liang W, Zhang Y, Shen Y, Tian X. Berberine regulates the Notch1/PTEN/PI3K/AKT/mTOR pathway and acts synergistically with 17-AAG and SAHA in SW480 colon cancer cells. *Pharm Biol*. 2021;59(1):21–30. doi:10.1080/13880209.2020.1865407

Pharmacogenomics and Personalized Medicine

Dovepress
Taylor & Francis Group

Publish your work in this journal

Pharmacogenomics and Personalized Medicine is an international, peer-reviewed, open access journal characterizing the influence of genotype on pharmacology leading to the development of personalized treatment programs and individualized drug selection for improved safety, efficacy and sustainability. This journal is indexed on the American Chemical Society's Chemical Abstracts Service (CAS). The manuscript management system is completely online and includes a very quick and fair peer-review system, which is all easy to use. Visit http://www.dovepress.com/testimonials.php to read real quotes from published authors.

Submit your manuscript here: https://www.dovepress.com/pharmacogenomics-and-personalized-medicine-journal